Traumatic Brain Injury at Multiple Length Scales: Relating Diffuse Axonal Injury to Discrete Axonal Impairment

R.J.H. Cloots[1], J.A.W. van Dommelen[1], S. Kleiven[2], M.G.D. Geers[1]

1 Eindhoven University of Technology, Department of Mechanical Engineering
PO Box 513, 5600 MB Eindhoven, The Netherlands
2 Division of Neuronic Engineering, School of Technology and Health,
Royal Institute of Technology, SE-141 52 Huddinge, Sweden

ABSTRACT

he length scales involved in the development of diffuse axonal injury, typically range from the head level (i.e., mechanical loading) to the cellular level, where discrete axonal injuries are located near inclusions. The aim is to investigate the local axonal strains near an inclusion in relation to the tissue level strains of the brain stem during mechanical loading of the head and the resulting orientation dependence of tissue level injury criteria. For this, a multi-scale FE approach is adopted. The results show that the axonal strains cannot be trivially correlated to the tissue strain without taking into account the axonal orientations, which indicates that the heterogeneities at the cellular level play an important role in brain injury and reliable predictions of it.

Keywords: DIFFUSE AXONAL INJURY, INJURY CRITERIA, HEAD MODEL, FINITE ELEMENT METHOD, MULTI-SCALE

THE BRAIN is a vulnerable part of the human body in case of an accident, such as in a road traffic crash situation. In Europe, which has a total population of 330 million people, about 50,000 people die because of traumatic brain injury (TBI) each year (Tagliaferri *et al.*, 2006). Diffuse axonal injury (DAI) is one of the most frequently occurring types of TBI (Gennarelli *et al.*, 1982). It is primarily involved with dynamic non-contact loading, although it is believed to occur in closed head impacts as well (Gentleman *et al.*, 1995; Smith *et al.*, 2003).

In order to improve the prevention or diagnosis of TBI, a better understanding of the relation between mechanical loading and TBI is necessary. Therefore, brain injury criteria are developed that can predict TBI as a results of a mechanical load. The most used brain injury criterion in the automotive industry nowadays is the head injury criterion (HIC), which is based on head level kinematics (Versace, 1971). Although the mechanical loading occurs at the head level, injury of the brain is often the result of more local mechanical phenomena. Because of this, more sophisticated brain injury criteria would account for these local mechanics. For this purpose, three-dimensional finite element (FE) head models are developed that simulate the response of a mechanical loading of the head to predict the possibility of TBI (e.g., Kleiven, 2007; Marjoux *et al.*, 2008; Takhounts *et al.*, 2003; Zhang *et al.*, 2004). FE head models have a good potential to predict DAI, since they describe local deformations within the brain (Miller *et al.*, 1998; Smith *et al.*, 2003). However, a well-defined correlation between mechanical loading and DAI using FE head models has not been achieved yet. A possible explanation is that the gyri and sulci in the brain, which are not included in these FE head models, can play an important role in the local tissue deformations (Cloots *et al.*, 2008; Ho and Kleiven, 2009; Lauret *et al.*, 2009). Furthermore, in case of DAI, the mechanical loading imposed on the head results in damage of the brain at the cellular level, which is influenced by heterogeneities within the tissue. Although from a macroscopic viewpoint, this type of injury has a diffuse appearance, from a microscopic viewpoint, it has been found that DAI is concerned with discrete focal damage of axons. According to Povlishock (1993), axonal injury is observed only at locations where the axons have to deviate from a straight path because of an obstruction (e.g., a blood vessel). This indicates that those axons might be subjected to locally higher strains than the tissue level strains, because of mechanical heterogeneities at the axonal level. Furthermore, it indicates that a region with axons near a blood vessel can be considered as a critical region for axonal injury. Moreover, in his experiments, Povlishock has found axonal damage mainly within the brain stem. Also,

other studies concerning TBI have shown that tissue strains can lead to injury at a cellular level (e.g., Bain *et al.*, 2001; Engel *et al.*, 2005; Floyd *et al.*, 2005; Morrison III *et al.*, 2006). This influence of the microstructure of the tissue might possibly lead to an orientation dependence of the sensitivity of brain tissue to a mechanical load in regions where the tissue has a unidirectionally oriented structure, indicating the importance of a coupling of tissue level brain injury criteria to microstructural aspects of the tissue.

Within this context, the aim of this study is to investigate the local axonal strains near a blood vessel in relation to the tissue level strains of the brain stem during mechanical loading of the head. To achieve a coupling between FE head models that do not contain details at a cellular level and cellular based injury criteria, a multi-scale framework with a macroscopic FE head model and a microscopic critical volume element (CVE), which is also modeled with an FE approach, is used. The CVE is based on the microscopic pathological findings for DAI.

METHODS

In this study, an existing FE head model (Kleiven, 2007) is used of which the loading conditions are based on the reconstruction of a real sports accident. A CVE representing a critical region for local axonal injury has been developed and is used in conjunction with this FE head model (see Figure 1). The loading conditions of the CVE are obtained from tissue deformations at specific locations within the head model. This results in axonal loading taking the orientation of the axons into account. Also, a situation is simulated in which no blood vessel is considered by taking the strain in the head model in the main axonal direction. Since the discrete focal impairments of the axons are found mainly in the brain stem, as mentioned in the previous section, focus is put on this part of the head model. In order to perform an in-depth study of the axonal strains in the CVE with respect to the tissue strains in the brain stem of the head model, one specific loading case of the head model is considered, where for each element of the brain stem a CVE simulation is performed. Furthermore, an anisotropic CVE is developed separately from the head model to investigate the influences of anisotropic mechanical properties caused by axonal orientations on the axonal loading.

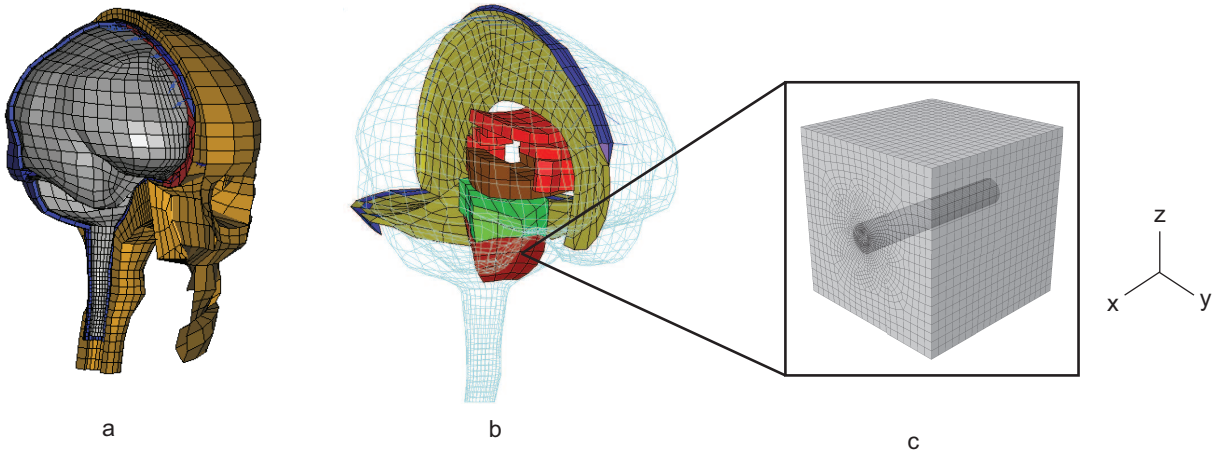

Figure 1: Models at different length scales: a) head model, b) head model showing several internal components and c) critical volume element. The x, y, and z-direction correspond to the lateral, the anterior-posterior, and the superior-inferior direction of the head, respectively.

HEAD MODEL: The head model that is used in this study is developed by Kleiven (2007) in the FE code LS-DYNA 971 (LTSC, Livermore, CA) and it consists of 11158 eight-node hexahedral elements, 10165 four-node shell and membrane elements, and 22 two-node truss elements. The material behavior of the brain stem in the head model is described by a linear viscoelastic model in combination with a

second order Ogden hyperelastic constitutive model. For the loading condition, the reconstruction of case 157H2 (Kleiven, 2007) is used, which is an injurious head impact loading case of a sports accident in the American National Football League (see Figure 2).

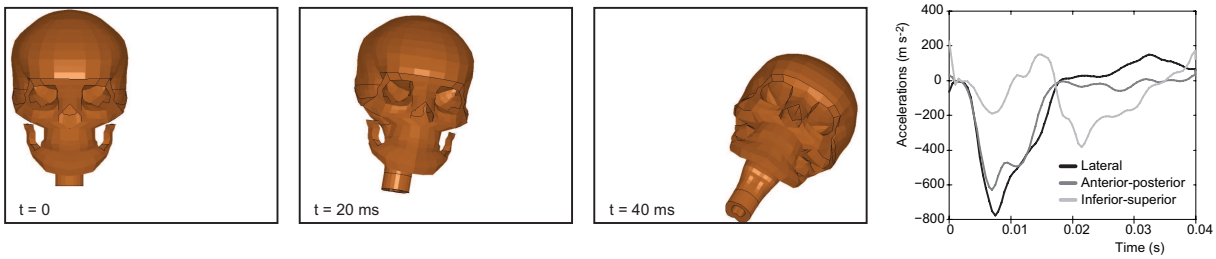

Figure 2: Head model loading condition based on the reconstruction of a struck sports player (concussed, HIC=472).

CRITICAL VOLUME ELEMENT: The CVE is developed using the FE code Abaqus 6.8-2 (Simulia, Providence, RI). It contains 27960 eight-node reduced integration hexahedral elements. The geometry of the CVE is based on pathological observations for axonal injury. It contains a blood vessel represented by a cylinder with a cross-sectional diameter of 8 μm and its surrounding material is assumed to consist of axons only. The blood vessel is oriented in either the lateral or the anterior-posterior direction as shown in Figure 1. The blood vessel and the surrounding tissue are assumed to be fully compatible at the interface. The tissue, consisting of axons, is modeled with a continuum approach. In line with the head model used at the macroscopic level, an isotropic Ogden model is used with the same properties as the head model (Kleiven, 2007). Note that the amount of critical locations is assumed to be small, so that the tissue properties at the microstructural level are assumed to correspond with those of at the macroscopic level. Although the tissue is modeled with isotropic material behavior, in order to obtain the axonal strains, each material point has a specific orientation representing the local axonal orientation, which is depicted in Figure 3. For all locations in the brain stem, the main axonal direction is in the z-direction, corresponding to the inferior-superior direction in the head model.

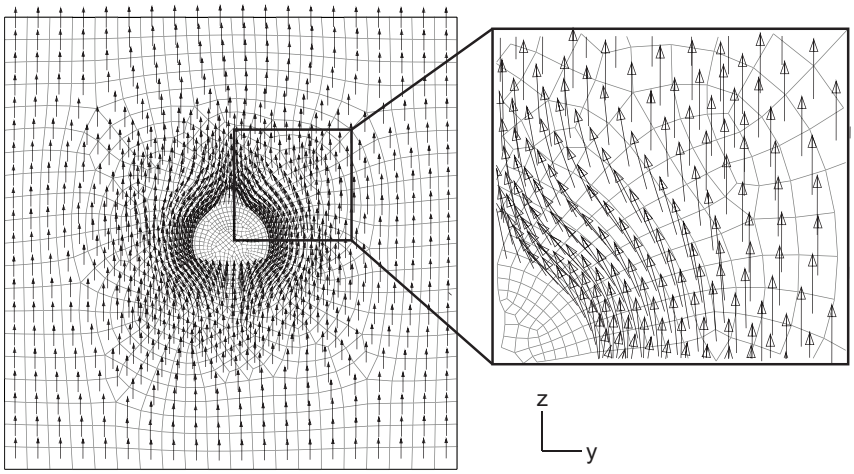

Figure 3: Front view of the CVE with the spatial discretization and the axonal orientation in each element of the part that consist of axons.

Also the behavior of the blood vessel is described with and Ogden model. The material properties of the blood vessel taken relative to those of the brain tissue: A) equal to those of the brain tissue, B) three times stiffer, and C) ten times stiffer. The results of the simulations with the blood vessel stiffness

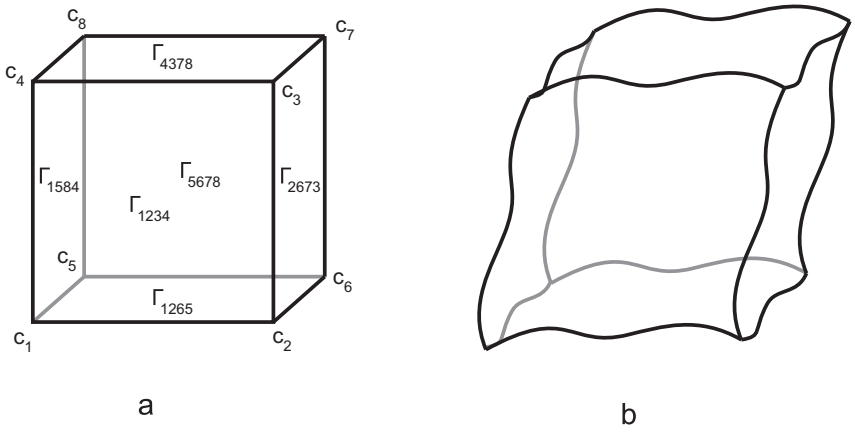

Figure 4: CVE with a) labeling of the corners and faces in the undeformed state and b) deformed model with periodic boundary conditions.

A will give insight into the influence of only the axonal orientations near a blood vessel on the axonal strain, whereas the blood vessel stiffnesses B and C will also show the influence of the heterogeneities in material stiffness at this level. All the material properties are shown in Table 1.

Table 1: Material properties of the CVE.

	Brain tissue	Blood vessel		
		A (1x)	B (3x)	C (10x)
μ_1 (Pa)	15.8	15.8	47.4	158
μ_2 (Pa)	-106.8	-106.8	-320.4	-1068
α_1	28.1	28.1	28.1	28.1
α_2	-29.5	-29.5	-29.5	-29.5
G_1 (kPa) for $\beta_1 = 10^6$ s^{-1}	484	484	1450	4840
G_2 (kPa) for $\beta_2 = 10^5$ s^{-1}	117	117	351	1170
G_3 (kPa) for $\beta_3 = 10^4$ s^{-1}	9.30	9.30	27.9	93.0
G_4 (kPa) for $\beta_4 = 10^3$ s^{-1}	12.0	12.0	36.0	120
G_5 (kPa) for $\beta_5 = 10^2$ s^{-1}	1.61	1.61	4.83	16.1
G_6 (kPa) for $\beta_6 = 10^1$ s^{-1}	4.44	4.44	13.3	44.4

The loading conditions of the CVE are obtained from the deformation gradient tensor of a specific element of the head model and are imposed by means of periodic boundary conditions (Kouznetsova *et al.*, 2001). The displacement vector $\vec{u}$ of a corner node c_i, as shown in Figure 4, is calculated from the global deformation gradient tensor $\bar{\boldsymbol{F}}$:

$$\vec{u}_{\mathrm{c}_i} = (\bar{\boldsymbol{F}} - \boldsymbol{I}) \cdot \vec{x}_{\mathrm{c}_i} \tag{1}$$

in which $\vec{x}_0$ is the initial position vector and $\boldsymbol{I}$ is the unit tensor and is prescribed for corner nodes c_1, c_2, c_4, and c_5. The nodal vector displacements of the remaining parts of the boundary are tied as follows:

$$\vec{u}_{\Gamma_{5678}} - \vec{u}_{\Gamma_{1234}} = \vec{u}_{\mathrm{c}_5} - \vec{u}_{\mathrm{c}_1} \tag{2}$$
$$\vec{u}_{\Gamma_{2673}} - \vec{u}_{\Gamma_{1584}} = \vec{u}_{\mathrm{c}_2} - \vec{u}_{\mathrm{c}_1} \tag{3}$$
$$\vec{u}_{\Gamma_{4378}} - \vec{u}_{\Gamma_{1265}} = \vec{u}_{\mathrm{c}_4} - \vec{u}_{\mathrm{c}_1} \tag{4}$$

where Γ_{jklm} denote the faces of the model (see Figure 4). As a result of these kinematical boundary conditions, antiperiodicity of the tractions is satisfied (Kouznetsova *et al.*, 2001).

ANISOTROPIC CVE: The material behavior of the head model is isotropic and therefore the material behavior of the underlying CVE is chosen to be isotropic as well. However, in reality, anisotropy has been found in brain tissue, especially in the brain stem (Arbogast and Margulies, 1998, 1999; Hrapko *et al.*, 2008; Nicolle *et al.*, 2005; Ning *et al.*, 2006; Prange and Margulies, 2002). In order to investigate the effects of anisotropy on the local axonal strain values, an anisotropic CVE has been developed as well. The anisotropic material behavior is described by a simplified form of the Holzapfel-Gasser-Ogden strain energy potential (Gasser *et al.*, 2006):

$$W = G(\tilde{I}_1 - 3) + K\left(\frac{J^2-1}{4} - \frac{1}{2}\ln J\right) + \frac{k_1}{2}\langle\kappa(\tilde{I}_1 - 3) + (1-3\kappa)(\tilde{I}_4 - 1)\rangle^2 \tag{5}$$

where G is the shear modulus, K is the bulk modulus, $\tilde{I}_1$ is the first invariant of the isochoric right Cauchy-Green deformation tensor $\tilde{\boldsymbol{C}} = J^{-\frac{2}{3}}\boldsymbol{C}$ with $\boldsymbol{C}$ the right Cauchy-Green deformation tensor and $J = \det(\boldsymbol{F})$ is the volume ratio. Furthermore, $\tilde{I}_4 = \tilde{\boldsymbol{C}} : \vec{n}_0\vec{n}_0$ is the isochoric fourth invariant and $\vec{n}_0$ is the fiber direction vector in the reference configuration with unit length, k_1 is the scalar fiber stiffness, and κ is the dispersion of the fiber orientations around the preferred fiber direction $\vec{n}_0$. The material properties of the brain tissue in the CVE are derived from the experimental study of Ning *et al.* (2006) on the brain stem of a 4-week old pig. For the material behavior of the inclusion, the same material property values are used, except that the fibers are assumed to be randomly oriented (i.e., $\kappa = \frac{1}{3}$). The values of the material properties can be found in Table 2. To investigate the influence of the stiffness of

Table 2: Material properties of the anisotropic CVE.

	Brain tissue with axonal fiber orientation		Inclusion
	unidirectionally	randomly	
G (Pa)	12.7	12.7	12.7
k_1 (Pa)	121.2	121.2	121.2
κ	0	$\frac{1}{3}$	$\frac{1}{3}$

the inclusion, the material properties of the inclusion are varied with respect to those of the brain tissue, for which also brain tissue composed of randomly oriented fibers (i.e., $\kappa = \frac{1}{3}$) is considered.

Since a direct coupling of the existing head model containing isotropic brain tissue and the anisotropic CVE would be unrealistic, the anisotropic CVE is considered separately. An isochoric planar overall deformation is applied, in which the principal strain direction is varied (see Figure 5). This direction is indicated by the angle θ with respect to the global z-direction (i.e., inferior-superior direction) of the model that corresponds with the main axonal direction. The global deformation gradient tensor prescribed is then given by

$$\bar{\boldsymbol{F}} = \bar{\lambda}\vec{m}_1\vec{m}_1 + \frac{1}{\bar{\lambda}}\vec{m}_2\vec{m}_2 + \vec{m}_3\vec{m}_3 \tag{6}$$

in which $\bar{\lambda} = 1.01$ is the globally applied stretch ratio and the vectors $\vec{m}_i$ (for $i = 1, 2, 3$) can be expressed in terms of the Cartesian vectors $\vec{e}_j$ (for $j = x, y, z$) and the angle θ. These loading conditions are also used for simulations in which no inclusion and/or isotropy is considered. Since no deformation is applied in the axial direction of the blood vessel and since the cross-sectional geometry does not vary in this direction, the anisotropic CVE can be described by a 2D plane strain model.

For the simulations with the fiber-based 2D models, a relative measure of the axonal strain with respect to a global load measure is evaluated. The axonal strain ε is defined as the maximum logarithmic strain in the axonal direction, which is the material direction $\vec{n}_0$ for unidirectionally oriented axons and the maximum principal strain direction for randomly oriented axons. By taking the maximum principal tissue strain $\bar{\varepsilon} = \ln(\bar{\lambda})$, which is imposed on the boundaries, as the global load measure, the relative strain becomes $\tilde{\varepsilon} = \frac{\varepsilon}{\bar{\varepsilon}}$.

During realistic loading conditions responsible for DAI, the tissue deformation is strongly driven by stress, because of the inertial forces acting on the brain. Therefore, also the maximum local strain with

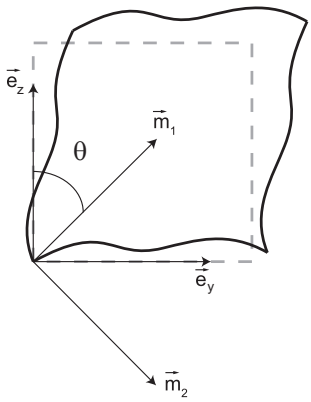

Figure 5: Isochoric deformation with the principal strain direction $\vec{m}_1$ and the main axonal direction along $\vec{e}_z$.

respect to the global normal stress difference of the tissue is considered, $\bar{\varepsilon}_\sigma = \frac{\varepsilon}{(\bar{\sigma}_{11}-\bar{\sigma}_{22})}$, where $\bar{\sigma}_{11}$ and $\bar{\sigma}_{22}$ are the homogenized stress components in the rotated coordinate system $\{\vec{m}_1,\vec{m}_2\}$, which are computed as in Kouznetsova *et al.* (2001). This normal stress difference corresponds to the maximum in-plane shear stress. Then, the axonal strain relative to the applied stress is normalized with this quantity for a reference situation, $\tilde{\varepsilon}_\sigma = \frac{\bar{\varepsilon}_\sigma}{\bar{\varepsilon}_{\sigma,\mathrm{ref}}}$, where the reference situation is the homogeneous fiber-reinforced tissue with unoriented axons.

RESULTS

MULTI-SCALE METHOD WITH HEAD MODEL AND CVE: From Figure 6, it becomes clear that the axonal strain has no clear relation to the tissue maximum principal strain for the simulations with and without a blood vessel. At some moments in time, the axonal strain remains small even though the tissue strain is large. Although in general, the axonal strains are lower than the corresponding tissue strains, it can be noticed that the presence of a blood vessel causes the difference between the axonal and tissue strain to decrease. For the case without a blood vessel, this difference is related to the angle φ between the tissue maximum principal loading direction and the main axonal direction, whereas this relation is not so clear for the simulations with a blood vessel. For the latter case, the orientation of the blood vessel strongly affects the trajectory in the graph of the axonal strain versus tissue strain.

The influence of the stiffness of the blood vessel on the maximum local axonal strain is displayed in Figure 7. The blood vessels A, B, and C have material properties that are equal to those of the brain tissue, three times higher, and ten times higher, respectively. Although the trajectory of the graph remains similar for all three cases, the maximum local axonal strain increases as the blood vessel stiffness relative to the brain tissue becomes higher.

Figure 8 shows the axonal strain field of the CVE with the blood vessel in the anterior-posterior direction with respect to the head. The tissue maximum principal strain is obtained at $t = 30$ ms, whereas the maximum axonal strain is much lower at that time. Although the tissue maximum principal strain is lower at $t = t_{\mathrm{end}}$, the maximum axonal strain in the CVE is higher than at $t = 30$ ms. One can also notice that the axonal strain values more distant from the blood vessel are in agreement with the strain values of the case without a blood vessel (see Figure 6).

When the axonal strain is plotted against the tissue maximum principal strain for all elements of the head model brain stem at each time step, a similar relation between the angle φ and the strain difference between tissue and axons is obtained for the situations without a blood vessel (see Figure 9). The results of the simulations with a blood vessel show only a small difference in axonal and tissue strain for a range of angles φ from 0° to about 40°. The axonal strains are never higher than their corresponding tissue maximum principal strains. However, it is also clear that the maximum principal strain observed in the tissue of the head model is not able to predict strains occurring at the axonal level.

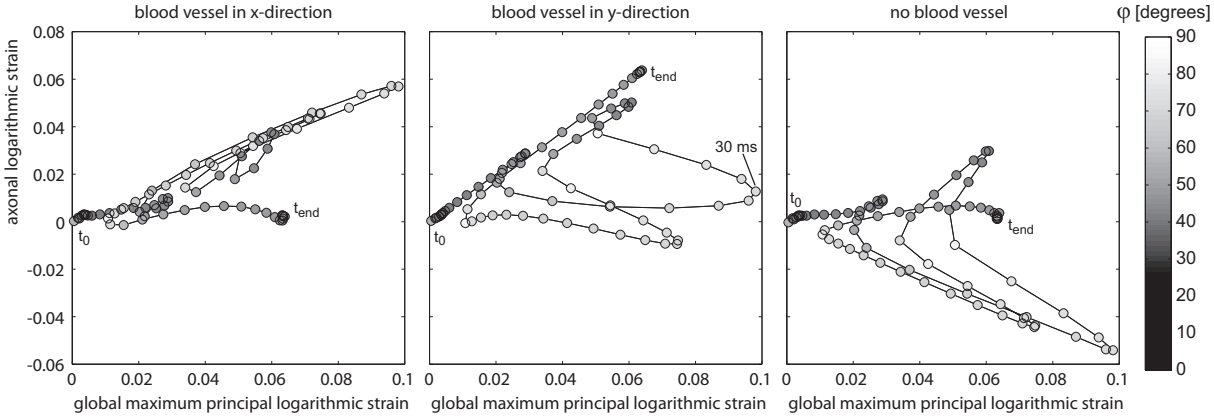

Figure 6: Maximum axonal strain in the CVE versus the tissue maximum principal strain at each time step from t_0 to t_{end} during the mechanical loading for the element of the brain stem in the head model with the highest tissue maximum principal strain. Angle φ denotes the angle between the tissue maximum principal loading direction and the main axonal direction.

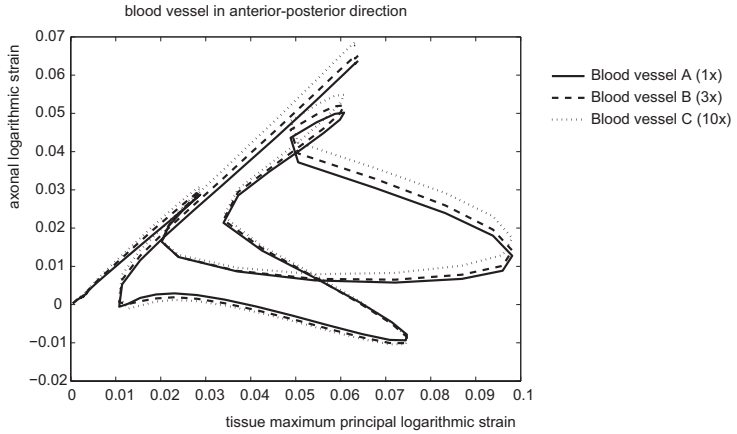

Figure 7: Maximum axonal strain in the CVE versus the tissue maximum principal strain at each time step from t_0 to t_{end} during the mechanical loading for the element of the brain stem in the head model with the highest tissue maximum principal strain.

Figure 10 depicts the axonal strain of the CVE versus the tissue strain of the head model in the main axonal direction for all elements of the brain stem. It can be noticed that the blood vessel causes the axonal strains to increase when the angle between the loading direction and the main axonal direction is large. Only for lower values of φ, the axonal strain is close to the corresponding tissue strain in the main axonal direction.

ANISOTROPIC CVE: In Figure 11, the maximum relative axonal strains, which were previously defined, are plotted as a function of the loading angle for the configurations with unidirectionally oriented fibers. The maximum axonal strain relative to the globally applied strain is about 1.2 for the situation with an inclusion. This value is obtained when the tissue is loaded in the main axonal direction. Large axonal strains are found for a small range of loading angles. At a loading angle of around $45°$, the tissue with the inclusion reaches a normalized maximum axonal strain relative to the applied stress that is 2.5 times the value obtained at the loading direction in the main axonal direction (i.e., $\theta = 0°$). For lower loading angles, the maximum strains relative to the applied stress are lower than for the 45° loading angle, because of the stiffening effect of the fibers that are oriented closely towards the loading angle.

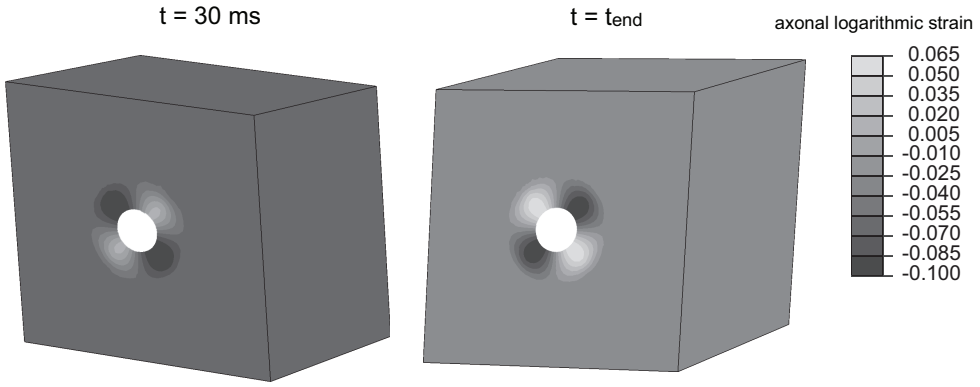

Figure 8: Axonal strain field of the CVE with the blood vessel in the anterior-posterior direction with respect to the head at $t = 30$ ms and $t = t_{\mathrm{end}}$. Note that the strain field of the blood vessel is not depicted for clarity.

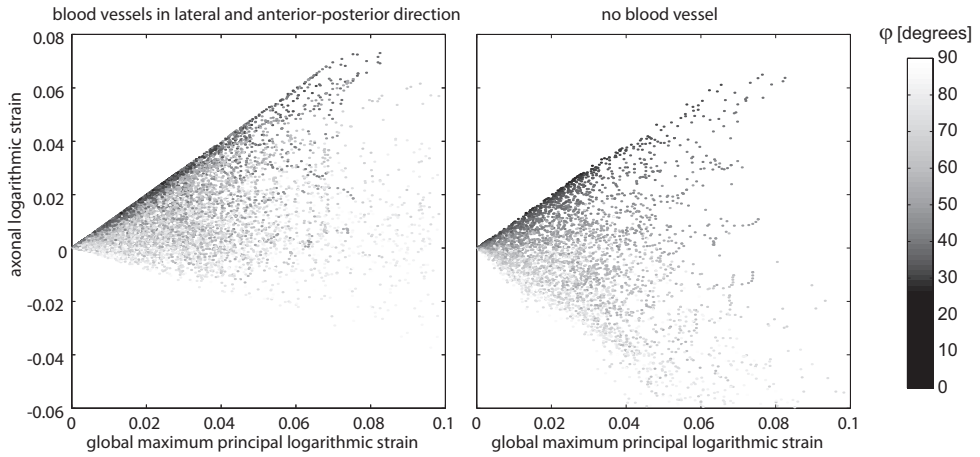

Figure 9: Maximum axonal strain in the CVE versus the tissue maximum principal strain at each time step during the mechanical loading for all elements of the brain stem in the head model. Angle φ denotes the angle between the tissue maximum principal loading direction and the main axonal direction.

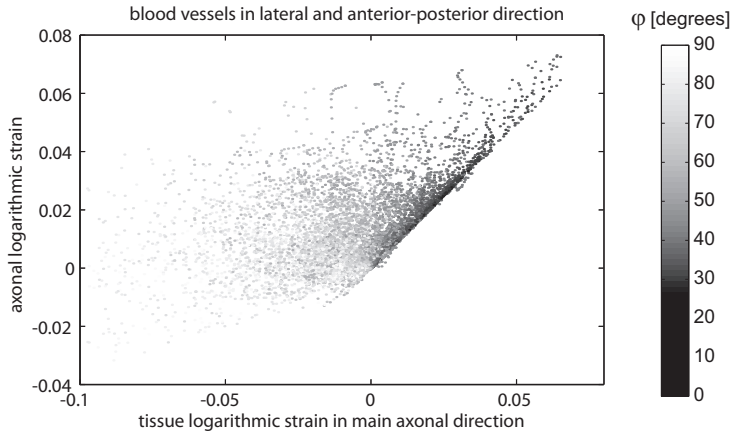

Figure 10: Maximum axonal strain in the CVE versus the maximum principal strain of the tissue at each time step during the mechanical loading for all elements of the brain stem in the head model. Angle φ denotes the angle between the tissue maximum principal loading direction and the main axonal direction.

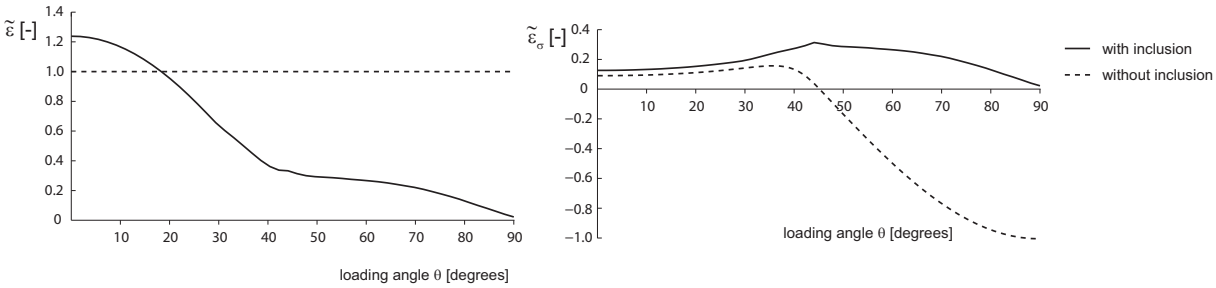

Figure 11: The maximum axonal strain relative to the applied tissue strain, $\tilde{\varepsilon}$, and the maximum axonal strain relative to the applied tissue stress, $\tilde{\varepsilon}_\sigma$, as a function of the principal loading angle θ for the anisotropic CVE.

For higher loading angles, the normalized strain relative to the applied stress decreases, because it is affected by the decrease of the axonal strain relative the applied strain. The configuration without an inclusion has a peak value for the relative strain at around $\theta = 36°$, with a value that is 1.7 times the value obtained at $\theta = 0°$. For higher loading angles, the axonal strain relative to the applied stress drops to lower values more rapidly compared to the model with inclusion.

The maximum axonal strain relative to the applied tissue strain is plotted against the relative inclusion stiffness in Figure 12, which is defined as $\frac{G_{inclusion}}{G_{tissue}} = \frac{k_{1,inclusion}}{k_{1,tissue}}$. For a high relative stiffness of the inclusion in the configuration with unidirectionally oriented fiber, the maximum axonal strain can exceed 1.7 times the global maximum principal tissue strain. This value is approximately 1.4 for the randomly oriented fiber configuration.

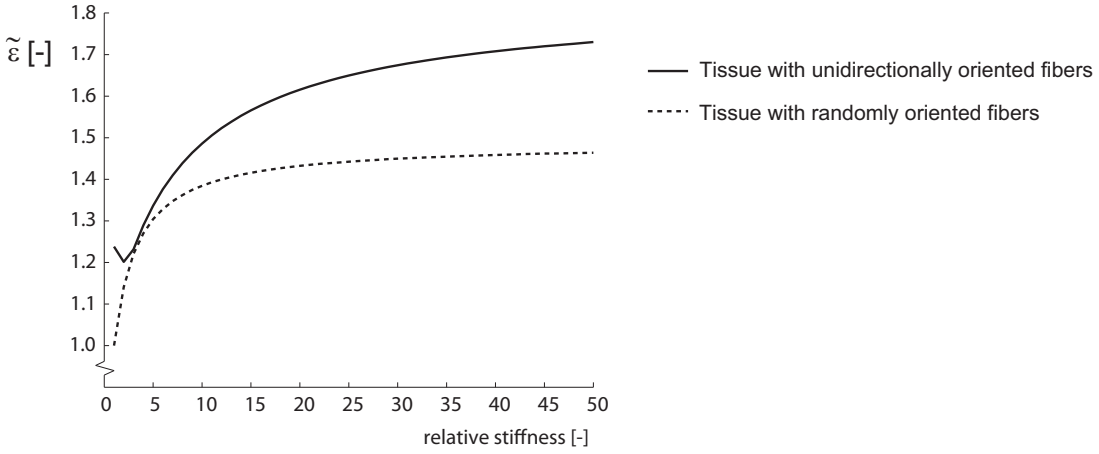

Figure 12: Axonal strain relative to the applied strain, $\tilde{\varepsilon}$, as a function of the stiffness of the inclusion with respect to the tissue stiffness at a loading angle of $\theta = 0°$.

DISCUSSION AND CONCLUSIONS

In this study, a multi-scale approach was used with a macroscopic FE head model to simulate the tissue response to mechanical loading and a micro mechanical FE model or CVE to obtain the local axonal strains due to the heterogeneities at the cellular level, which are assumed to be the cause of the discrete local axonal impairments in case of DAI. The strain values of the CVE and the FE head model have no trivial correlation, which indicates that the brain injury criteria for DAI should be developed at the cellular level instead of at the tissue level. Even more differences in the strains between the tissue and the cellular level might exist for more realistic material configurations (e.g., anisotropy or differences in

stiffness between inclusion and axons).

The FE head model has a geometry that distinguishes several parts of the brain (e.g., cerebral cortex, brain stem). Although it does not include a detailed geometry (e.g., sulci), the influence of these details are assumed to be local and therefore do not affect the tissue deformations of the brain stem. Although the brain stem in the model, in reality would be more cylindrically shaped, the total volume is close to MRI volumetric measurements of the brain stem for healthy volunteers.

The material properties of the head model are isotropic, whereas in reality areas of the brain with aligned axons show anisotropic material behavior (Arbogast and Margulies, 1998, 1999; Hrapko *et al.*, 2008; Nicolle *et al.*, 2005; Ning *et al.*, 2006; Prange and Margulies, 2002). Although this can have an effect on the macroscopic tissue deformations, the influence of the axonal orientation locally can still be obtained from the CVE with isotropic material behavior by means of the local strains in the axonal direction. Nevertheless, a separate CVE with anisotropic material properties is developed to find the influence of anisotropy on the local axonal strains. At the tissue level, the anisotropy causes the strain to become smaller in the main axonal direction. Therefore, also the axonal strains reduce for tissue strains in the main axonal direction. Although other loading directions result in higher tissue strains for the same stress, the axonal strain decreases, since the loading direction is not aligned with the axons anymore. Still, for the axons that have to deviate for an inclusion, this alignment exists for a wider range of loading directions than without an inclusion. Because of this, these axons have a higher strain locally caused by anisotropic material behavior.

The loading conditions of the FE head model are based on the reconstruction of one specific injurious sports accident using HIII dummies (Kleiven, 2007). Because of this, only the motion of the head could be applied to the head. Therefore, the possibly important influence of spinal cord bending could not be included in the analysis, which might affect the strain levels in the brain stem. Nevertheless, since this study is concerned with the maximum local axonal strains with respect to the tissue strains, the conclusions drawn from the results are expected to be relatively independent of the global mechanical load. In a future study, more loading cases, both injurious and without injury, have to be simulated to better investigate the relation of the axonal strains at the cellular level and the probability of brain injury.

The CVE has a geometry with a simplified blood vessel in only two different directions. It is expected that more realistic geometries give quantitatively different results for a single CVE simulation, but will show the same mechanisms to affect the sensitivity of brain tissue to a mechanical load as those observed in the current study.

Currently, the CVE is coupled only to the brain stem of the head model. Because also other parts of the brain can be involved with DAI, it is necessary to couple these parts as well. In general, axons in other parts of the brain are less aligned than in the brain stem. This will probably result in different axonal strains relative to the tissue strain than for the brain stem. Furthermore, the brain stem has a relatively simple geometry, whereas other parts of the brain might need more detailed geometries of the FE head model to obtain true tissue deformations.

This study shows that axonal strains can deviate from the tissue strains that are predicted in a FE head model. This is caused by the local heterogeneities at the cellular level, which are local axonal orientation, difference in stiffness between the axons and the inclusion, and anisotropic material behavior of the axons. The latter factor also influences the tissue strain in the FE head model. A tissue level mechanical output parameters obtained from the head model, such as the tissue maximum principal strain value and direction or the tissue strain in the main axonal direction, have no clear correlation to the maximum axonal strains in the CVE. Since DAI is a type of injury, in which the mechanical load occurs at the head level and the actual injury occurs at the cellular level, a multi-scale method with a FE head model and CVE is a promising approach to obtain cellular based injury criteria. However, ultimately, macroscopic head model simulations can account for the cellular level effects by merely applying these injury criteria.

ACKNOWLEDGEMENTS

This work has been supported by the Dutch Technology Foundation STW, applied science division of NWO and the Technology Program of the Ministry of Economic Affairs.

REFERENCES

Arbogast, K. B. and Margulies, S. S. (1998). Material characterization of the brainstem from oscillatory shear tests. *J Biomech*, 31:801–807.

Arbogast, K. B. and Margulies, S. S. (1999). A fiber-reinforced composite model of the viscoelastic behavior of the brainstem in shear. *J Biomech*, 32:865–870.

Bain, A. C., Raghupathi, R., and Meaney, D. F. (2001). Dynamic stretch correlates to both morphological abnormalities and electrophysiological impairment in a model of traumatical axonal injury. *J Neurotrauma*, 18:499–511.

Cloots, R. J. H., Gervaise, H. M. T., van Dommelen, J. A. W., and Geers, M. G. D. (2008). Biomechanics of traumatic brain injury: influences of the morphologic heterogeneities of the cerebral cortex. *Ann Biomed Eng*, 36:1203–1215.

Engel, D. C., Slemmer, J. E., Vlug, A. S., Maas, A. I. R., and Weber, J. T. (2005). Combined effects of mechanical and ischemic injury to cortical cells: secondary ischemia increases damage and decreases effects of neuroprotective agents. *Neuropharmacology*, 49:985–995.

Floyd, C. L., Gorin, F. A., and Lyeth, B. G. (2005). Mechanical strain injury increases intracellular sodium and reverses Na^{+}/Ca^{2+} exchange in cortical astrocytes. *Glia*, 51:35–46.

Gasser, T. C., Ogden, R. W., and Holzapfel, G. A. (2006). Hyperelastic modelling of arterial layers with distributed collagen fibre orientations. *J R Soc Interface*, 3:15–35.

Gennarelli, T. A., Spielman, G. M., Langfitt, T. W., Gildenberg, P. L., Harrington, T., Jane, J. A., Marshall, L. F., Miller, J. D., and Pitts, L. H. (1982). Influence of the type of intracranial lesion on outcome from severe head injury. *J Neurosurg*, 56:26–32.

Gentleman, S. M., Roberts, G. W., Gennarelli, T. A., Maxwell, W. L., Adams, J. H., Kerr, S., and Graham, D. I. (1995). Axonal injury: a universal consequence of fatal closed head injury. *Acta Neuropathol*, 89:537–543.

Ho, J. and Kleiven, S. (2009). Can sulci protect the brain from traumatic injury? *J Biomech*, 42:2074–2080.

Hrapko, M., van Dommelen, J. A. W., Peters, G. W. M., and Wismans, J. S. H. M. (2008). The influence of test conditions on characterization of the mechanical properties of brain tissue. *J Biomech Eng*, 130:031003–1–10.

Kleiven, S. (2007). Predictors for traumatic brain injuries evaluated through accident reconstruction. *Stapp Car Crash Journal*, 51:81–114.

Kouznetsova, V. G., Brekelmans, W. A. M., and Baaijens, F. P. T. (2001). An approach to micro-macro modeling of heterogenous materials. *Comp Mech*, 27:37–48.

Lauret, C., Hrapko, M., van Dommelen, J. A. W., Peters, G. W. M., and Wismans, J. S. H. M. (2009). Optical characterization of acceleration-induced strain fields in inhomogeneous brain slices. *Med Eng Phys*, 31:392–399.

Marjoux, D., Baumgartner, D., Deck, C., and Willinger, R. (2008). Head injury prediction of the HIC, HIP, SIMon and ULP criteria. *Accident Anal Prev*, 40:1135–1148.

Miller, R. T., Margulies, S. S., Leoni, M., Nonaka, M., Chen, X., Smith, D. H., and Meaney, D. F. (1998). Finite element modeling approaches for predicting injury in an experimental model of severe diffuse axonal injury. *Stapp Car Crash Journal*, 42.

Morrison III, B., Cater, H. L., Benham, C. D., and Sundstrom, L. E. (2006). An in vitro model of traumatic brain injury utilising two-dimensional stretch of organotypic hippocampal slice cultures. *J Neurosci Meth*, 150:192–201.

Nicolle, S., Lounis, M., Willinger, R., and Palierne, J. F. (2005). Shear linear behavior of brain tissue over a large frequency range. *Biorheology*, 42:209–223.

Ning, X., Zhu, Q., Lanir, Y., and Margulies, S. S. (2006). A transversely isotropic viscoelastic constitutive equation for brainstem undergoing finite deformation. *J Biomech Eng*, 128:925–933.

Povlishock, J. T. (1993). Pathobiology of traumatically induced axonal injury in animals and man. *Ann Emerg Med*, 22:980–986.

Prange, M. T. and Margulies, S. S. (2002). Regional, directional, and age-dependent properties of the brain undergoing large deformation. *J Biomech Eng*, 124:244–252.

Smith, D. H., Meaney, D. F., and Shull, W. H. (2003). Diffuse axonal injury in head trauma. *J Head Trauma Rehabil*, 18:307–316.

Tagliaferri, F., Compagnone, C., Korsic, M., Servadei, F., and Kraus, J. (2006). A systematic review of brain injury epidemiology in Europe. *Acta Neurochir*, 148:255–268.

Takhounts, E. G., Eppinger, R. H., Campbell, J. Q., Tannous, R. E., Power, E. D., and Shook, L. S. (2003). On the development of the SIMon finite element head model. *Stapp Car Crash Journal*, 47:51–57.

Versace, J. (1971). A review of the severity index. *Stapp Car Crash Journal*, 15.

Zhang, L., Yang, K. H., and King, A. I. (2004). A proposed injury threshold for mild traumatic brain injury. *J Biomech Eng*, 126:226–236.